Research Article

Journal of Environmental Nanotechnology

High Speed Flow Visualization of Primary Breakup Phenomenon of Pyrolysis Oil-diesel Blend Using Air-assisted Atomizer

Amar Malode[1], N. Tamilarasan[1], K. Balaji[1*] and R. Sakthivel[2]

[1]Department of Mechanical Engineering, Amrita School of Engineering, Amrita Vishwa Vidyapeetham, Coimbatore, TN, India
[2]Department of Mechanical Engineering, Government College of Technology, Coimbatore, TN, India
Received: 04.03.2024 Accepted: 19.06.2024 Published: 30.06.2024
*k_balaji@cb.amrita.edu

ABSTRACT

The energy crisis poses major difficulties for humanity, yet it also brings chances for innovation, sustainability, and a shift towards a more environmentally friendly and fairer future. Transforming waste into energy is a sustainable solution for a greener future. The present study focuses on energy generation through pyrolysis of 3-ply disposable polypropylene facemask. Thermogravimetric analysis, differential scanning calorimetry as well as proximate and ultimate analyses were conducted on the sample to identify compounds and thermal behavior of the sample. The activation energy of decomposition was calculated through a chemical kinetic study using 3 different methods, Kissinger-Akahira-Sunose, Ozawa-Flynn-Wall, and Starink model and was found out to be 178.17, 190.06 and 178.67 kJ, respectively. Thermodynamic properties like enthalpy, entropy, Gibbs free energy was determined to be 132.661, -0.01712, 143.019 kJ/mol. Highly viscous pyrolysis-oil and char were produced through pyrolysis process. The spray generated using an air-assisted atomizer measured the combustion. Miniature air assisted atomizer was designed and fabricated for high-speed flow visualization. The experimentation part of the study was carried out using high speed camera (10,000 frames per second) and the results were processed and analyzed for determination of breakup length, spray angle, critical wavelength and breakup frequency. The study suggests that the advanced synthetic fuel (pyrolysis oil- diesel blend) generated from facemask could become a potential source of energy production adhering to waste to energy strategy.

Keywords: Pyrolysis oil-diesel blend; Atomization; Thermal analysis; Entropy; Enthalpy; Gibbs free energy.

1. INTRODUCTION

As the world continues to face the challenges of climate change and depleting fossil fuel resources, the search for sustainable energy solutions becomes more critical than ever. One promising avenue is the conversion of waste into energy, which not only helps to alleviate the burden on landfills but also provides a renewable energy source to meet our growing needs. The COVID-19 pandemic has impacted waste generation globally, requiring the attention of policymakers to address the fluctuations and challenges in solid waste management, particularly with biomedical, plastic, and food waste (Sharma *et al.* 2020). The majority of the medical trash is made up of 3-ply face masks, which are mostly made of highly volatile substances, mainly comprising of polypropylene (PP) (Jahirul *et al.* 2012; Matsuzawa *et al.* 2001). These facemasks can be decomposed using pyrolysis treatment as well as generate bio-oil (energy) from the same, which may be a suitable alternative for common combustion fuels (Azam *et al.* 2012). Pyrolysis of surgical mask layers generates a carbon-rich, oxygen-deficient liquid oil with a high heating value, offering environmentally beneficial waste-to-energy upcycling to combat plastic pollution (Li *et al.* 2022; Sakthivel *et al.* 2023). The main objective of this research was to produce pyrolysis oil using 3-ply disposable COVID-19 facemasks as the source material. Additionally, the study aims to develop a blend by combining the resulting bio-oil with a predetermined quantity of bio-diesel (Nileshkumar *et al.* 2015). The experiments were conducted using an air-assisted atomizer. This study estimated the activation energy of decomposition through a comprehensive chemical kinetic analysis employing three distinct approaches: the Kissinger-Akahira-Sunose (KAS) method, the Ozawa-Flynn-Wall (OFW) method, and the Starink model. Additionally, an assessment and comparison of essential thermodynamic properties, such as enthalpy, entropy, and Gibbs free energy, were conducted (Clifford Ishola *et al.* 2023).

Pyrolysis is a process that decomposes biomass without oxygen, producing combustible gases and bio char. It yields bio-oil, bio-char, and syngas, with proportions influenced by feedstock and processing conditions. In pyrolysis of waste surgical masks, high oil yield with minimal gaseous and calcium-rich char products was obtained at 500°C (Yousef *et al.* 2022; Tamilarasan *et al.* 2022; Tamilarasan *et al.* 2023). High rate of feeding and higher rate of gas flow resulted in high amount of pyrolysis-oil yield. When pyrolysis-oil was

heated above 500℃, it formed one homogenous phase instead of the two different phases (Asadullah *et al.* 2013). Pyrolysis of the main organics in waste surgical masks (polypropylene) occurs at temperature range of 250–650℃ (Li *et al.* 2022; Mondal, 2022; Yousef *et al.* 2022).

Atomization is the process of breaking large liquids into smaller droplets to increase surface area and evaporation rates. It is used in products like shower heads and deodorant sprays. High-speed flow visualization helps understand and optimize spray processes in industries like automotive, aerospace, and pharmaceutical, leading to advancements in fuel combustion and drug delivery systems. High-speed spray characterization provides valuable insights into atomized liquids, aiding in optimizing processes and enhancing efficiency. It enables the development of computational models for various applications, including fuel combustion and drug delivery systems. To visualize highly viscous fuel sprays, appropriate lighting, optics, spray generation methods, and image analysis techniques are essential, along with safety considerations. High-speed spray visualization finds applications in fuel injection systems, industrial processes, environmental impact studies, alternative energy research, aerospace applications, and fuel development. Advanced synthetic fuels, like e-fuels, offer carbon neutrality, energy storage, compatibility with existing infrastructure, and fuel diversity, presenting a promising solution to address challenges associated with traditional fossil fuels (Mangesh *et al*. 2020).

Multiple studies have examined various aspects of thermal breakdown, pyrolysis, and atomization processes. Researchers have investigated the kinetics and byproducts of propylene's thermal breakdown, the interaction of different compounds during pyrolysis, and the effects of pyrolysis temperature on oil yield and phase separation. Other studies have focused on characterizing pesticide spray properties, evaluating the performance of pyrolysis reactors, analyzing chemical bonds in organic materials using FTIR analysis, and addressing challenges and opportunities in plastic waste pyrolysis. The potential of pyrolysis for energy and resource recovery from waste materials, such as face masks and surgical gloves, has also been explored. These studies contribute to our understanding of these processes and their applications.

Szwarc, (1949) investigated propylene's thermal breakdown, observing homogeneity in the gas reaction of the first order, discussing two byproducts and their kinetics-explaining mechanisms. Matsuzawa *et al*. (2001) studied the pyrolysis of various compounds separately and in mixtures, noting the influence of PVC and PVdC on cellulose degradation, producing more char at lower temperatures (Matsuzawa *et al.* 2001; Jahirul *et al*. 2012) summarized over two hundred publications on pyrolysis technology for biofuel production, emphasizing the importance of biomass selection for high bio-oil yields. Higher pyrolysis-oil yield at elevated temperatures and the formation of a homogenous phase above 500℃ was found with phenol being a prominent component in palm kernel shell pyrolysis (Asadullah *et al.* 2013). Minov *et al*. (2015) employed high-speed imaging techniques to characterize pesticide spray and non-intrusively assess droplet properties. Khachani *et al*. (2015) used isoconversional techniques to study multi-step thermal decomposition, separating different processes with the Fraser-Suzuki equation.

Balaji *et al*. (2018) characterized interfacial instability in liquid jets and sheets using high-speed flow visualization techniques. Martynis *et al*. (2019) evaluated a 125 dm^3 pyrolysis reactor, obtaining liquid fuel with properties comparable to kerosene and gasoline. Organic materials were analyzed using FTIR, providing a valuable resource for interpreting FTIR peaks in biochemical studies (Nandiyanto *et al.* 2019). Qureshi *et al*. (2020) explored opportunities and challenges in plastic waste pyrolysis, emphasizing the importance of feedstock quality and pre-treatment. Ghasemi *et al*. (2020) studied breakup processes in air-assisted atomization of pyrolysis oils, revealing intricate two-phase interactions. Focused on characterizing primary atomization using a co-flowing air configuration and advanced flow visualization methods. Park *et al*. (2021) examined co-pyrolysis of food waste and single-use face masks, exploring energy and resource recovery. Kristanto *et al*. (2021) developed a kinetic model for multi-step biomass pyrolysis, using DTG and DSC findings to support the thermodynamic characteristics in kinetic modeling. Panchasara and Ashwath, (2021) reviewed the effects of pyrolysis bio-oils on fuel atomization, emphasizing the need for standardized fuel characteristics and improved combustion. The pyrolysis kinetic behavior of coronavirus facemasks using TG-FTIR system was investigated (Yousef *et al.* 2021). Aragaw and Mekonnen, (2021) discussed sustainable plastic waste management and converting facemasks into bio-oils due to their thermoplastic nature. Key factors impacting product yields in pyrolysis of waste polypropylene plastics, highlighting the advantages of slow pyrolysis was reviewed (Harussani *et al.* 2022). Li *et al*. (2022) proposed using used surgical masks as fuel and energy feedstocks during pyrolysis to reduce plastic pollution. Pyrolysis and catalytic cracking of facemasks, converting them into liquids and light hydrocarbons was explored (Sun *et al.* 2022). Yousef *et al.* (2022) found that optimal oil output and minimal gas and char formation during pyrolysis at 500℃, significantly impact the economy.

From the broad literature review, it is clear that there are limited studies relevant to spray characterization of biodiesel blend which is obtained from pyrolysis oil. Atomization is crucial in many applications such as combustion of fuels, powder metallurgy, etc. COVID-19

has resulted in production of huge amount of waste, majority of which is 3-ply use and throw facemasks (Amiruzzaman *et al*. 2022). This study will help in finding an optimized way to dispose the facemasks through pyrolysis treatment as well as generate pyrolysis oil through it. Also, the sources of conventional fuels are getting depleted due to continuous overuse. The pyrolysis oil when blended with bio-diesel may be a cheaper and sustainable alternative for the combustion fuels which is renewable (Akbulut and Yalniz, 2022).

2. MATERIALS AND METHODS

Polypropylene is the main component of 3-ply face masks, known for its excellent filtration properties. Polypropylene samples for analysis were obtained by shredding masks. Thermogravimetric Analysis (TGA) was used to assess the mass loss of the sample as the temperature changes, providing information on its degradation and reaction kinetics. Proximate analysis determined the moisture, volatile matter, fixed carbon, and ash content of the sample, while ultimate analysis examined the elemental composition. Pyrolysis of the shredded masks generated highly viscous pyrolysis oil, which was blended with diesel using a surfactant catalyst for further experimentation. Fourier Transform Infrared (FTIR) analysis was employed to identify the chemical composition of materials based on their infrared absorption patterns. Surfactants were used to enhance the homogeneity of the oil-diesel blend.

2.1 Materials and Sample Preparation

The 3-ply disposable facemask is primarily made of polypropylene, a thermoplastic polymer known for its excellent filtration properties, making it ideal for facial coverings. The mask's melt-blown layer contains densely packed fibers that effectively capture and filter tiny particles like bacteria, viruses, and contaminants. Polypropylene has a chemical formula of $(C_3H_6)_n$ and a density ranging from 0.895 to 0.92 g/cm^3. To obtain a sample of PP, the nose and ear straps were removed from 250 facemasks purchased from a medical shop. These masks were then dried for 12 hours in sunlight to reduce their moisture content. The dried facemasks were shredded into pieces measuring 1 mm to 4 mm in length using scissors to create the sample. The total weight of the shredded facemasks from the 250 pieces was found to be 560 g, as shown in Fig. 1. Subsequently, the shredded facemask samples underwent TGA, DSC analysis, proximate, and ultimate analyses separately. The test results were then studied using thermodynamics and chemical kinetics to estimate parameters such as activation energy, enthalpy, entropy, and so on.

Fig. 1: Chopped facemask sample

2.2 Proximate Analysis

The method of determining the presence and quantity of various substances in a mixture is known as proximate analysis. Proximate analysis involves the measurement of moisture, volatile matter, fixed carbon, and ash using specific procedures. The biomass should equal the total of all the components. When a PP sample is heated to 450°C in a nitrogen environment, kept there, and then the atmosphere is changed to air, the mass loss that occurs as a result is measured (Stevovic *et al*. 2023).

2.3 Ultimate Analysis

The process of identifying the various chemical components contained in a certain substance is known as

ultimate analysis. The last examination checks the sample's carbon, hydrogen, nitrogen, sulphur, and oxygen concentration to ascertain its elemental makeup.

2.4 Thermogravimetric Analysis

Thermogravimetric analysis is a technique where a sample's mass is continuously assessed as the temperature varies (Nasrollahzadeh *et al.* 2019). It is frequently used to assess specific properties of materials that experience mass loss or gain as a result of oxidation, breakdown, or the loss of volatiles. This analysis is frequently used to characterize materials by examining distinctive breakdown patterns, to study degradation processes and reaction kinetics, and to determine the amount of organic material in a sample (Salin and Seferis, 1993). The primary elements of the device comprise a customizable furnace and an extremely responsive scale employed to gauge variations in the weight of the sample. The scale is thermally insulated to prevent interference from the heat of furnace. A thin wire hangs down from the scale into the furnace, and at the bottom of the wire, the sample tray is positioned to ensure consistent results. To enhance the sensitivity, accuracy, and precision of weighing, it is crucial to shield the balance from heat influences, such as by utilizing a temperature-controlled chamber. Infrared spectrometry can be employed alongside TGA to analyze and identify gases generated during sample deterioration. Modern TGA equipment typically includes a computer that calculates the weight-loss fraction or percentage. Commercial TGA devices are capable of reaching temperatures exceeding 1000°C, possess a balancing sensitivity of 0.1 µg, and allow for controlled heating rates in an air or gas environment. The TGA can heat up at a rate ranging from 0.1 to 200 °C per minute (Ebnesajjad, 2011).

2.5 Pyrolysis Oil GENERATION

Fig. 2 (a) shows the pyrolysis experimental setup used for the study. The chopped dry facemask pieces about 1-4 mm in length were fed in the pyrolysis reactor which was then flushed with nitrogen gas to get rid of any air present and create a vacuum chamber. The pyrolysis reactor was held in a combustor which starts heating the sample. The pyrolysis of biomass typically occurs at around 500°C. The raw gases travel to a chamber where char and remaining exhaust gases are separated. After separation of char, the gases were then quenched in cool water to get the bio-oil whereas the gases which cannot be condensed travel back to the combustor and help in the combustion process. The pyrolysis oil generated was highly viscous. Fig. 2 (b) shows the generated pyrolysis oil.

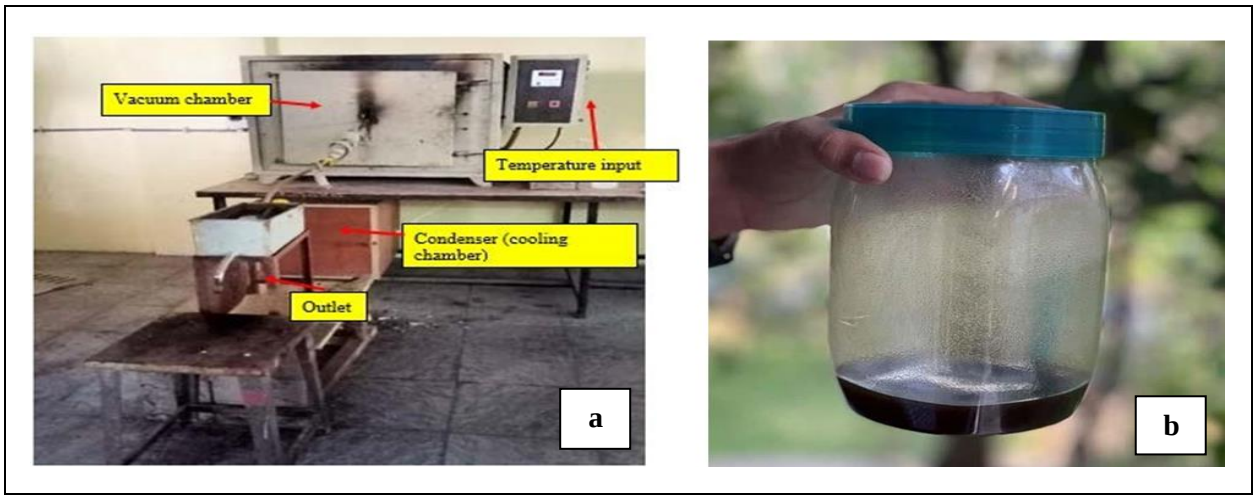

Fig. 2: (a) Pyrolysis experimental setup (b) Generated pyrolysis oil

The pyrolysis process produced pyrolysis oil which was collected in a beaker, and its quantity amounted to around 350 mL. The yield of propylene pyrolysis was determined to be 31.11%.

2.6 Fourier Transform Infrared (FTIR) Analysis

The FTIR analysis is a widely employed technique in analytical chemistry for the identification and characterization of chemical composition of materials. This analysis is based on the principle that molecules selectively absorb infrared radiation at frequencies specific to their chemical structure. By measuring the sample's infrared absorption, FTIR provides insights into the material's chemical bonds and functional groups (Matsuzawa *et al.* 2001).

2.7 Blending

The samples were then blended with diesel for further experimental spray visualization. Blending of the oil with diesel requires surfactant to be added as a catalyst

to make the blend homogenous. A surfactant, in its uniquely distinctive and original form, can be defined as a specialized compound or substance that exhibits exceptional surface-active properties. Fig. 3 (a) shows tween 80 and Span 80 surfactants used for the study. It possesses a distinctive ability to reduce the surface tension of a liquid, thereby enabling it to spread or disperse efficiently over various interfaces.

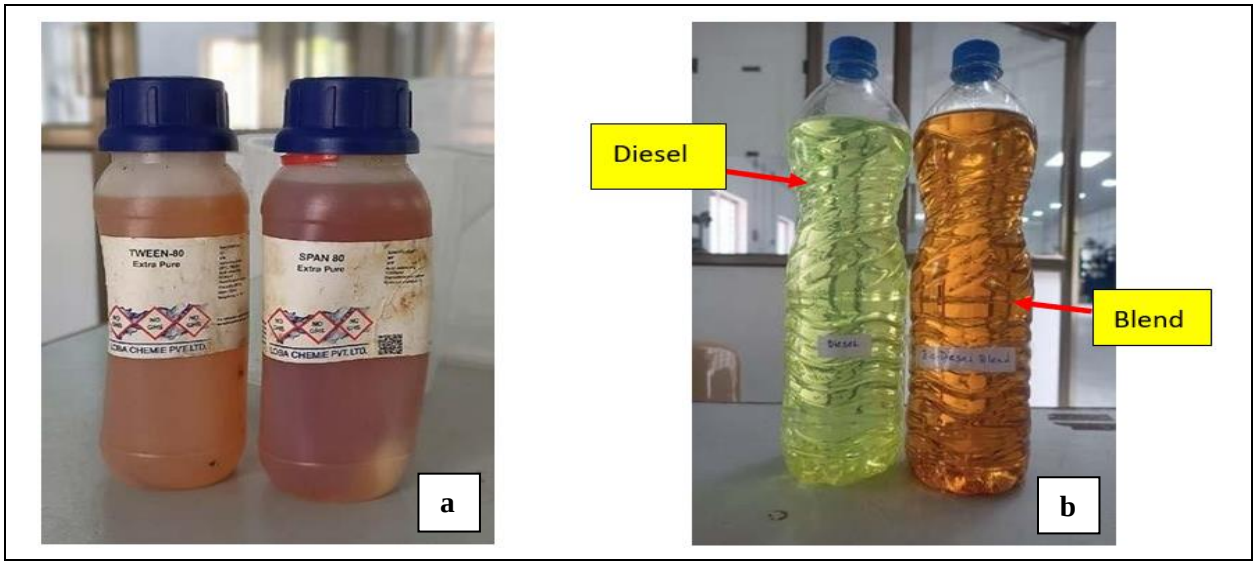

Fig. 3: (a) TWEEN 80 and SPAN 80 surfactants, (b) Diesel and blend

Having originality and uniqueness, surfactants play a crucial role in various fields, including detergents, cosmetics, pharmaceuticals, and industrial processes, where their unrivaled surface-active properties are utilized to achieve desired outcomes with unparalleled effectiveness. Fig. 3 (b) shows diesel and biodiesel blend. A homogenous blend was achieved using the surfactants TWEEN-80 and SPAN-80 by mixing them with oil-diesel blend in the ratio 0.2:10 *i.e.* 20 mL of surfactant per 100 mL of oil-diesel blend.

2.8 Miniature Atomizer Design

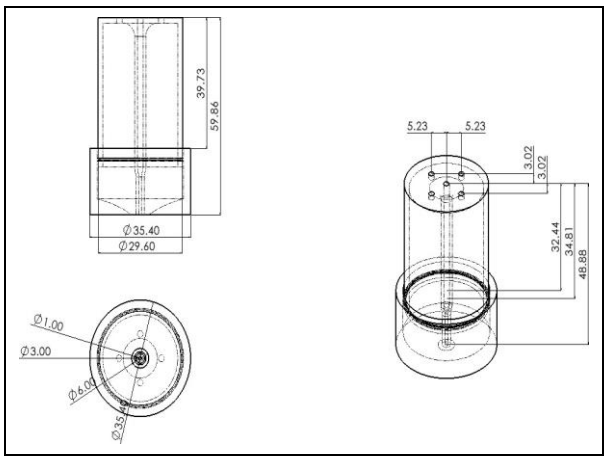

Fig. 4: Miniature atomizer design

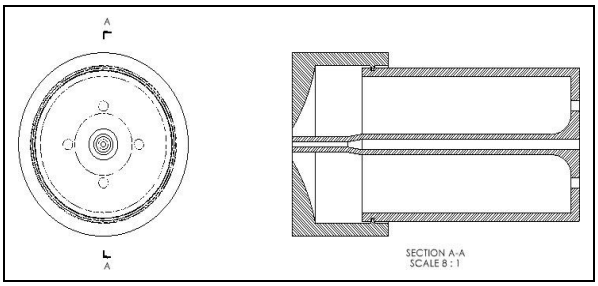

Fig. 5: Sectional view of the miniature atomizer

Miniature atomizer was designed to conduct flow visualization (Fig. 4). The model was designed in Solid works 2022 software which is widely used in the industry for 3D modelling purposes. All dimensions are in mm. Actual design of atomizer was studied and to make it into miniature size, the dimensions were converted based on ratio 3:1 and also certain curvatures and lengths were dimensionalized based on literature survey of atomizer design. The sectional view of the model is shown in Fig. 5.

2.9 Atomizer Fabrication

The fabrication process involves 3D printing of air assisted atomizer. The model has been printed using the Creality CR-10 3D printer with PLA (polylactic acid thermoplastic) material. Fig. 6 shows the 3D printed atomizer.

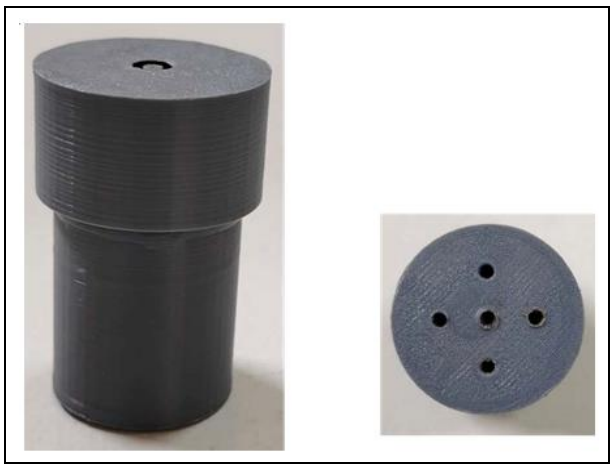

Fig. 6: Fabricated atomizer

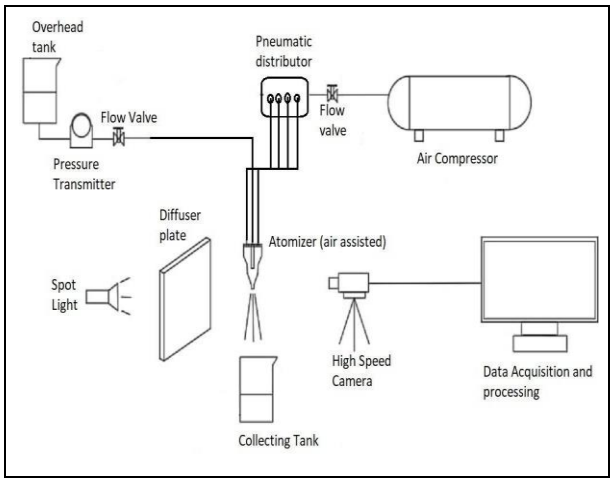

Fig. 7: Experimental setup layout

2.10 Experimental Setup

The experimental setup was prepared as shown in Fig. 7. The pneumatic distributor in the layout was used before the atomizer to channel the air flowing from the air compressor to the inlet of atomizer. The experimentation is conducted in dark environment to get accurate results. High speed camera capable of capturing 1,44,000 fps was used to visualize the spray diffuser plate. The spot light enabled the camera to capture high quality images of the spray. Fig. 8 shows the experimental setup used for the study. Air pressure and liquid velocity was regulated using flow valve which allows to capture results at different pressure and velocity. Results were obtained from data acquisition unit connected to the high-speed camera. The results were processed and primary instability variables were calculated manually.

2.11 Flow Visualization

In the flow visualization studies, a LED source with a power of 37 W was employed. The high-speed camera used for image capture was the Photron Fastcam Mini UX50 from West Wycombe, UK, with an acquisition rate of 10,000 fps. For capturing the images, a Nikon lens with a focal length of 50 mm and an aperture of 1:12 was utilized. To feed the bio-diesel to the atomizer, 0.2 mm diameter PVC tubes were used, connected to an overhead tank. The flow of bio-diesel through the PVC tubes was controlled using a roller flow controller clamp. The collected bio-diesel was manually recycled back to the overhead tank. The atomizer received air supply from an air compressor, which was regulated using a needle valve. This ensured a controlled and consistent air flow for the atomization process.

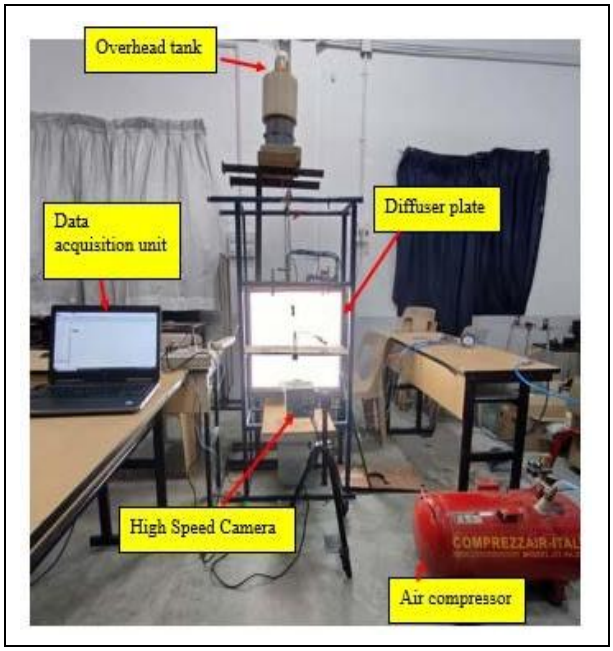

Fig. 8: Experimental setup

3. RESULTS AND DISCUSSION

The thermal breakdown of face masks occurs between 400°C and 500°C, with different heating rates affecting the process. The activation energy for decomposition was determined using three different methods, and thermodynamic properties were also analyzed. The face masks have a high volatile content and carbon composition. The use of surfactant as a catalyst in blending proves effective for creating homogeneous blends. FTIR analysis helps identify functional groups in the oil and char. Atomization studies show that air velocity affects breakup length and spray angle. The pyrolysis oil-diesel blend exhibits properties similar to petroleum diesel but with some differences. This study explores the potential of pyrolysis oil-diesel blend as an alternative fuel.

3.1 Proximate and Ultimate Analysis

The proximate analysis result shows (Table 1) that 94.07% of the sample is volatile *i.e* more susceptible

to change. For proximate analysis the standard test methods used are ASTM-D3172, ASTM-D3174, ASTMD3175.

For ultimate analysis to determine the elemental composition, the test methods used are ASTM-D3178, ASTM-D3179, ASTM-D3177. The result of the ultimate analysis shows (Table 2) that percentage of carbon content is high in the sample *i.e* 83.78% along with negligible amounts of sulphur and oxygen.

Table 1. Proximate analysis

Sample	Moisture %	Volatile content %	Ash %	Fixed Carbon
Polypropylene (facemasks)	3.45	94.07	1.79	0.69

Table 2. Ultimate analysis

Name	Content (%)				
	C	H	N	S	O
Polypropylene (facemask)	83.78	15.24	0.000	0.200	0.78

3.2 TGA

DSC and TGA results show the weight percentage (mass) and heat flow change with temperature and time when the 3-ply facemask sample is heated linearly with time for it to thermally decompose. The weight loss curve obtained from measurements provides valuable information regarding the following aspects:

Alterations in the composition of the sample:

- Thermal stability of the sample.
- Kinetic variables associated with chemical reactions occurring in the sample.
- The derivative weight loss curve indicates the optimum degradation temperature, which corresponds to the temperature at which weight loss is most pronounced.

Thermal analysis gives the information with changes in mass. This analysis has applications in characterization of thermal studies and material purity and also examination of corrosion studies and gasification processes.

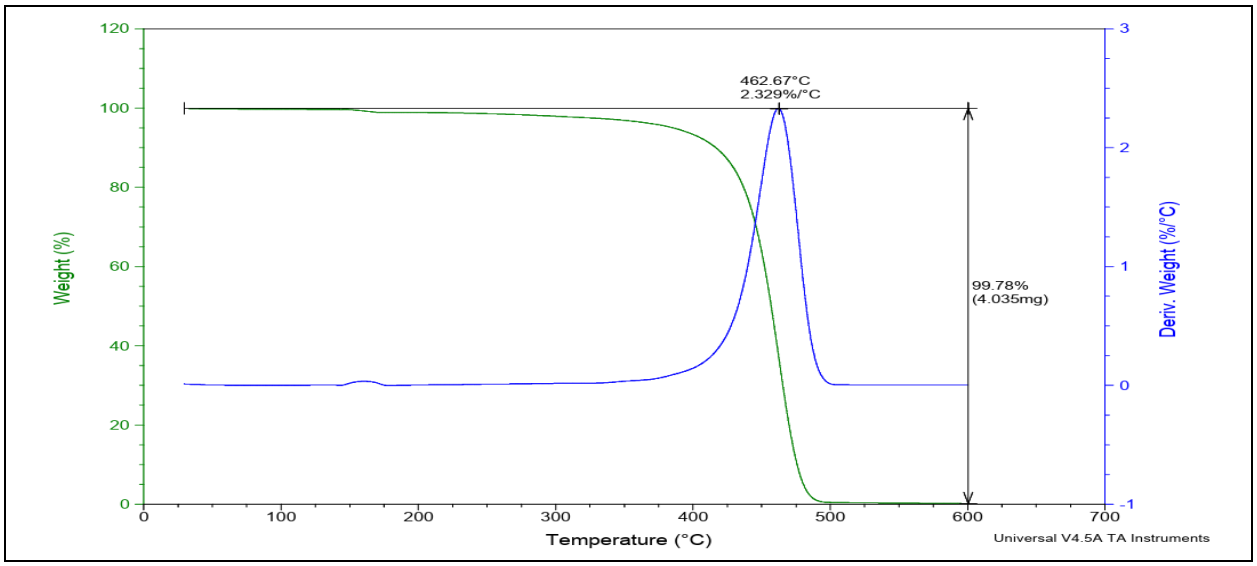

Fig. 9: DSC-TGA plot for sample at heating rate 5℃/min

From Fig. 9, it can be inferred that, for the linear heating rate of 5 ℃/min, the decomposition of the facemask sample starts around 400℃ and was completely decomposed at around 475℃. The sudden decrease in the curve indicates rapid conversion of the sample into product. Weight loss of the sample was found to be 99.62% *i.e*. 99.62% of sample is fully decomposed. The derivative weight curve shows the optimum degradation temperature at 440.70℃ with 2.317%/℃ as the derivative weight. Fig. 10 indicates that the disintegration of the facemask sample begins around 375℃ and was completed at about 490℃ for the linear heating rate of 10℃/min. The curve shows an abrupt decline indicating quick turning of sample into product. It was determined that 99.89% of the sample had lost weight, or was entirely degraded. The derivative weight curve indicates that the ideal temperature for deterioration is 455.15℃, with a derivative weight of 2.346%/ ℃.

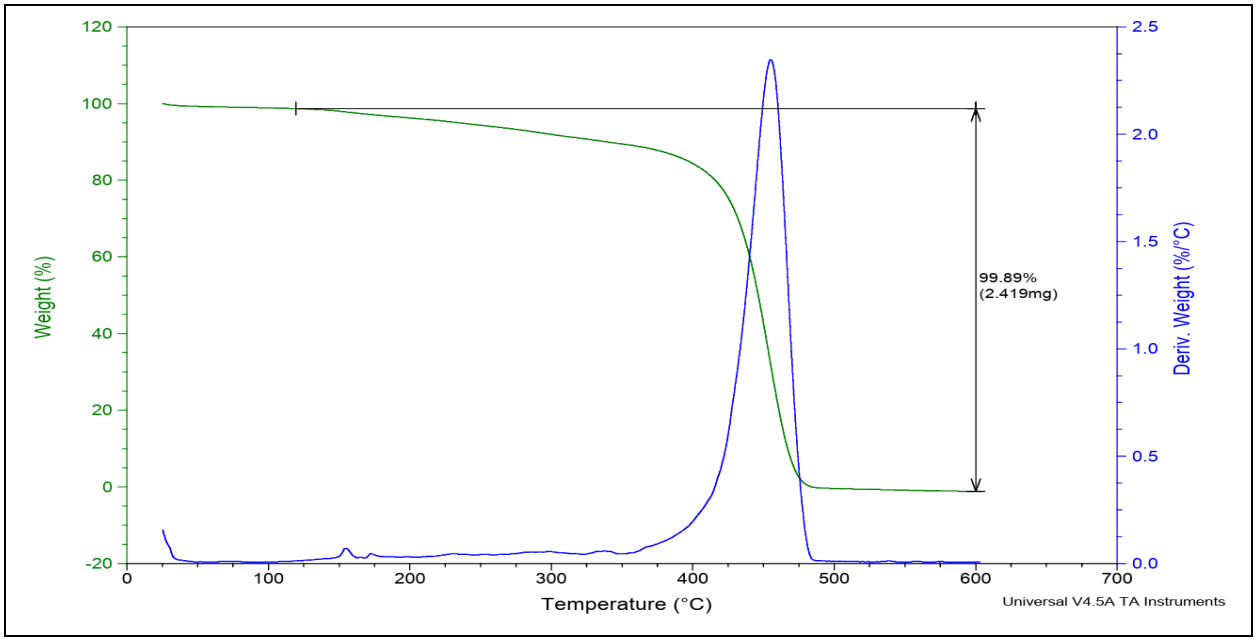

Fig. 10: DSC TGA plot for sample at heating rate 10 °C/min

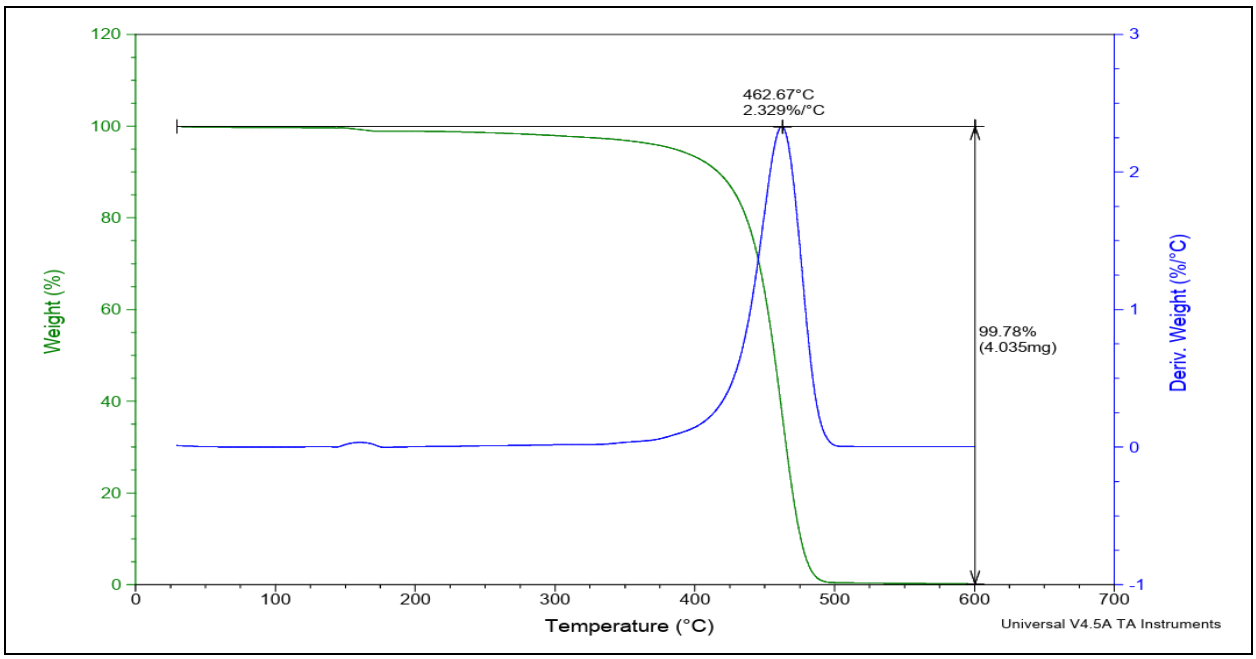

Fig. 11: DSC TGA plot for sample at heating rate 15°C/min

From Fig. 11, it is inferred that for the linear heating rate of 15°C/min, the decomposition of the facemask sample starts around 410°C and is completely decomposed at around 500°C. The sudden decrease in the curve shows rapid conversion of the sample into product. 99.78% of sample was fully decomposed. The derivative weight curve shows the optimum degradation temperature at 462.67°C with 2.329%/°C as the derivative weight.

The plot shown in Fig. 12 indicates that the disintegration of the facemask sample around 415 °C and the completion was at 490 °C for the linear heating rate of 20 °C/min. The curve's abrupt decline indicates the quick conversion of sample into product. It was determined that 99.56% of the sample had lost weight, or was entirely degraded. The derivative weight curve indicates that the ideal temperature for deterioration being 469.20 °C, with a derivative weight of 2.449%/ °C.

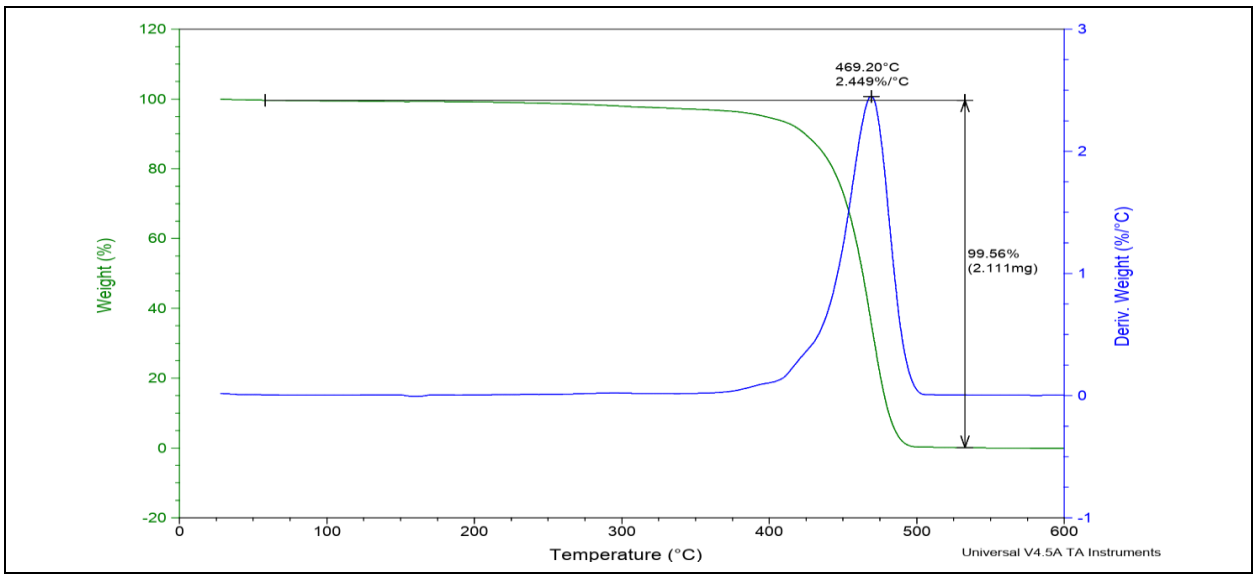

Fig. 12. DSC-TGA plot for sample at heating rate 20 °C/min

3.3 Estimation of Activation Energy

Activation energy is the minimum amount of energy needed for a sample to undergo a conversion into a product, making it a crucial parameter to be determined. The kinetic parameters linked to this procedure, namely the apparent activation energy (Ea), frequency factor (A), and reaction model (f(α)), are collectively known as the kinetic triplet. These factors are determined using different model-free isoconversional techniques, such as the Kissinger-Akahira-Sunose method, Ozawa-Flynn-Wall method, and Starink model. These methods enable the estimation of the kinetic parameters without relying on a specific reaction model or mechanism.

When it comes to the thermal degradation of biomass, its kinetics are assumed to follow a multiple-step process, but for practical purposes, they can be effectively approximated as a single-step reaction. This simplification allows for a more convenient representation of the biomass pyrolysis reaction in terms of the conversion of biomass substrate into yield. The relation for this conversion can be expressed as shown in equation (1).

$$\frac{d\propto}{dt} = k(T)f(\propto) - - - - - - - - - - (1)$$

By applying the aforementioned kinetic triplet and utilizing the appropriate model-free iso-conversional methods, researchers can gain valuable insights into the thermal behavior of biomass and accurately predict its degradation patterns.

In the equation, the term dα/dt represents the degree of biomass conversion, while f(α) represents the reaction model, which is a function that relies on the physical and chemical properties associated with the process. The conversion ratio (α) is defined as:

$$\propto = \frac{w_0 - w_t}{w_0 - w_f} - - - - - - - - - - (2)$$

In the context of the biomass pyrolysis reaction, several variables play a crucial role. In the given equation (2), the variable "w_0" represents the initial mass of the biomass sample at time (t) = 0. The variable "w_t" represents the mass of the biomass sample at a specific time (t) during the decomposition process, and "w_f" represents the mass of the biomass sample at the end of the decomposition process. These variables can be determined by collecting continuous data through thermogravimetric analysis performed on the biomass sample. This analysis enables the measurement of mass changes as a function of temperature or time, providing valuable insights into the thermal behavior of the biomass. Moreover, the reaction rate (k(T)) can be calculated using the Arrhenius equation. The Arrhenius equation establishes a connection between the reaction rate, temperature, and two significant factors:

$$k(T) = Ae^{\left(\frac{-Ea}{RT}\right)} - - - - - - - - - - - - (3)$$

In the equation (3), k (T) represents the reaction rate at a specific temperature (T), Ea is the apparent activation energy, A is the frequency factor, and R is the gas constant. By applying the Arrhenius equation, researchers can assess the influence of temperature on the reaction rate and gain insights into the kinetics of the biomass pyrolysis process. Substituting these values and assuming a linear heating rate, equation (4) is obtained, as shown below:

$$\frac{d\propto}{dT} = \frac{A}{\beta}e^{\left(\frac{-Ea}{RT}\right)}f(\propto) - - - - - - - - - - (4)$$

Integral form of above equation can be written as shown in equation (5).

$$g(\propto) = \int_0^{\propto} \frac{d \propto}{f(\propto)} = \frac{A}{\beta}\int_{T0}^{T} e^{\left(\frac{-Ea}{RT}\right)} dT$$
$$= \frac{AE_aT^2}{\beta} e^{\left(\frac{-Ea}{RT}\right)} - - - - - - (5)$$

The solution to the equation (6) can be obtained through numerical computation or by expressing the reaction progress function, g(α), using an approximate equation. In the KAS model, the solution is expressed as follows:

$$ln\frac{\beta}{T^2} = ln\frac{AR}{g(\alpha)} - \frac{Ea}{RT} - - - - - - - - - - - (6)$$

There are various methods to estimate the activation energy based on the Arrhenius equation. However, the Kissinger and the Starink method are the most accurate. Fig.13 shows kinetic parameter analysis plot by KAS isoconversional model.

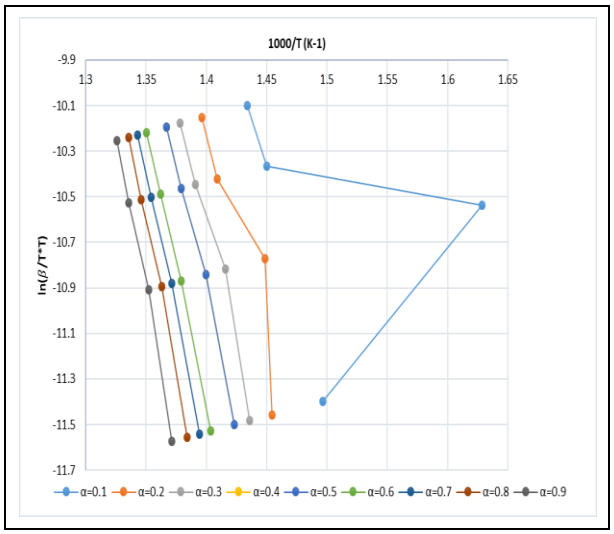

Fig. 13: Kinetic parameter analysis by KAS isoconversional model

The Ozawa-Flynn-Wall (OFW) technique is a model-independent method employed to determine the activation energy and frequency factor of a substance. It utilizes Doyle's approximation to estimate these parameters. The OFW method is utilized to ascertain the kinetic properties of a substance without assuming a specific reaction mechanism. It is particularly advantageous when the reaction mechanism is unknown or intricate. By employing the OFW method, scientists can examine the thermal degradation behavior of a substance and compute its activation energy and frequency factor. These parameters offer valuable insights into the substance's thermal stability, reactivity, and potential applications. Doyle's approximation is employed in the OFW method to simplify the calculation process. It assumes a constant reaction order and a single heating rate, enabling a more straightforward determination of the activation energy and frequency factor.

Equation (7) to estimate the activation energy by OFW method is given below:

$$Ln(\beta) = Ln\left(\frac{A * Ea}{R * g(\propto)}\right) - 5.331 - 1.052\frac{Ea}{R * T} - - - - - - (7)$$

The activation energy was calculated by plotting slope -1.052 Ea/(R*T) of graph between Ln(β) and 1/T. Fig. 14 shows kinetic parameter analysis plot by OFW isoconversional model.

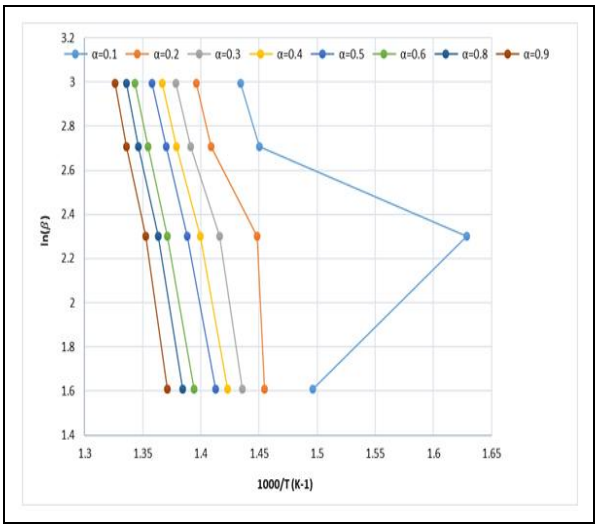

Fig. 14: Kinetic parameter analysis by OFW isoconversional model

The Starink model is a non-isothermal, model-free method that sets itself apart from the KAS and OFW models. Unlike the KAS and OFW models, the ST (Starink) method does not provide a single kinetic parameter and instead relies on the conversion value. Research has shown that the ST method offers higher accuracy. Fig. 15 shows kinetic parameter analysis plot by Starink model. The unique aspect of the ST method lies in its dependence on the conversion value. This means that the accuracy of the method can be enhanced by carefully selecting an appropriate conversion value for analysis. By considering the specific conversion level, the ST method offers improved precision in determining the activation energy of a reaction. The ST model is valued for its higher accuracy, making it a reliable tool for studying the kinetics of various processes and reactions. The equation for Starink method which is derived from approximations can be written as shown in equation (8):

$$ln\left(\frac{\beta}{T^{1.8}}\right) = C_s - 1.0037\left(\frac{E}{RT}\right) - - - - - - - (8)$$

The activation energy was calculated by plotting a linear graph between ln β/($T^{1.8}$) and 1/T. The preexponential factor was calculated using expression (Criado *et al.* 2008), as shown in equation (9):

$$A = \frac{\beta E_a e^{\left(\frac{E_a}{RT}\right)}}{RT^2} \text{ – – – – – – – – – – – (9)}$$

Table 3 shows a comparison of apparent activation energy values for various conversion ratio by KAS, OFW and Starink models.

Table 3. Activation energy and R2 values using different isoconversional model-free methods for kinetic analysis

Conversion ratio (α)	KAS		Starink		OFW	
	Ea (kJ/mol)	R^2	Ea (kJ/mol)	R^2	Ea (kJ/mol)	R^2
0.1	12.0586256	0.0517	12.4926164	0.0553	22.900082	0.1635
0.2	147.299138	0.8235	147.764722	0.8245	158.95537	0.8447
0.3	180.12281	0.8235	180.596708	0.8245	191.937	0.9723
0.4	190.091296	0.9907	190.565194	0.8245	202.01357	0.9918
0.5	197.382674	0.9962	197.864886	0.9962	209.38809	0.9966
0.6	203.219102	0.9971	203.701314	0.9971	215.29103	0.9974
0.7	211.865662	0.9965	212.356188	0.9965	224.01242	0.9969
0.8	223.363924	0.994	223.85445	0.994	235.5855	0.9946
0.9	238.129588	0.9903	238.628428	0.9904	250.45925	0.9913
Average	**178.170313**	**0.8515**	**178.647167**	**0.833667**	**190.06026**	**0.883233**

The average activation energy (Ea) obtained from the KAS, OFW, and Starink methods was found to be 178.17 kJ/mol, 190.06 kJ/mol, and 178.64 kJ/mol, respectively (Fig. 13 -15). The corresponding R^2 values obtained for these methods were 0.85, 0.88, and 0.83, indicating the goodness of fit for each method.

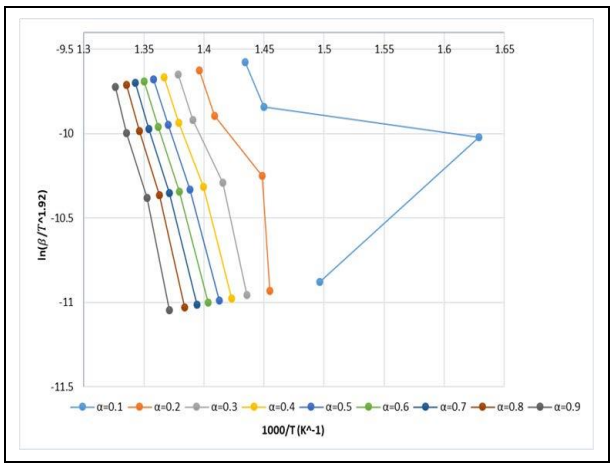

Fig. 15: Kinetic parameter analysis by Starink model

The OFW method consistently yields higher activation energies at all conversion ratios, while the activation energies for KAS and Starink are fairly comparable (Fig. 16). The OFW method offers a better fit for the data than KAS and Starink, according to the R^2 values, which points to a stronger correlation between the conversion ratio and activation energy. While the exact relationship can vary between methods, in general, as the conversion ratio rises, the activation energy also tends to rise.

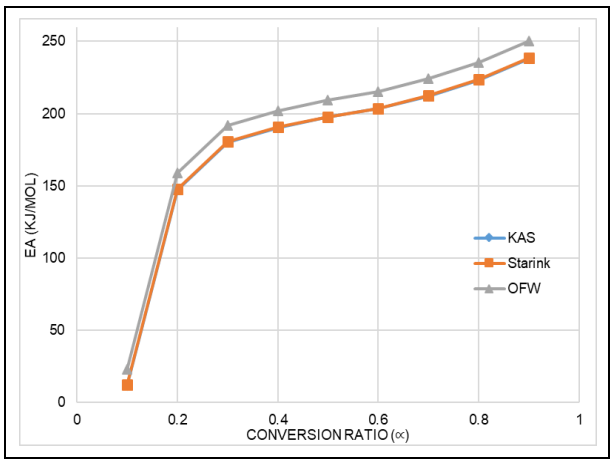

Fig. 16: Activation energy vs Conversion ratio comparison

3.4 Thermodynamic Analysis

Based on kinetic parameters (Ea and A) the thermodynamic parameters are determined as shown in equation (10), equation (11) and equation (12):

$$Enthalpy, (\Delta H) = E_a - RT \text{ – – – – – – – – (10)}$$

$$Entropy, (\Delta S) = Rln\frac{Eh}{KT} \text{ – – – – – – – – – – (11)}$$

$$Gibbs\ free\ energy, (\Delta G) = \Delta H - T\Delta S \text{ – – – – (12)}$$

Where: h is Planck's constant 6.62607015 × 10^{-34} m^2 kg/s, K is Boltzmann's constant (1.380649 × 10^{23} $m^2kgs^{-2}K^{-1}$). The relationship between thermodynamic parameters can be utilized to effectively elucidate the various phases involved in biomass decomposition. The calculation of changes in enthalpy (ΔH) and Gibbs free

energy (ΔG) values for different models provide insights into their variations.

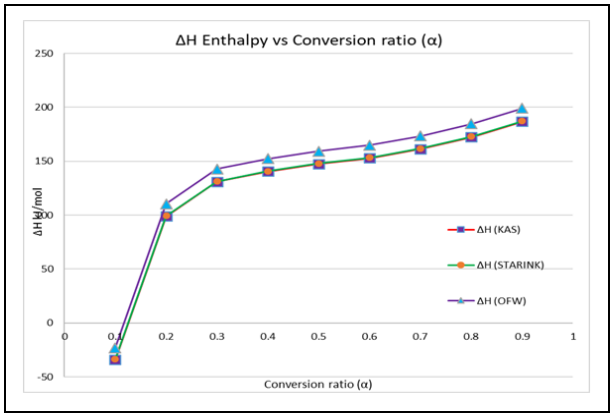

Fig. 17: Enthalpy vs conversion ratio comparison

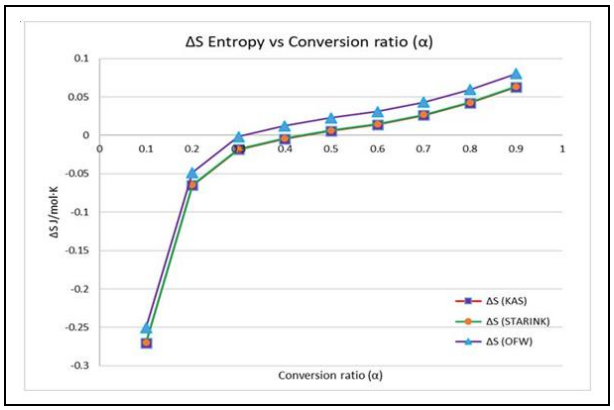

Fig. 18: Enthalpy vs conversion ratio comparison

The average values offer a comprehensive understanding of the overall alterations in entropy, enthalpy, and Gibbs free energy across various conversion rates for each method (Fig.17 – Fig. 19 and Table 4).

KAS: The values for ΔS, ΔH, and ΔG for KAS range from negative to positive values across different conversion rates. For example, at a conversion rate of 0.1, ΔS is approximately -0.271, ΔH is -34.066 kJ/mol, and ΔG is 146.646 kJ/mol. The average values for KAS indicate an average ΔS of -0.023, an average ΔH of 128.539 kJ/mol, and an average ΔG of 143.206 kJ/mol.

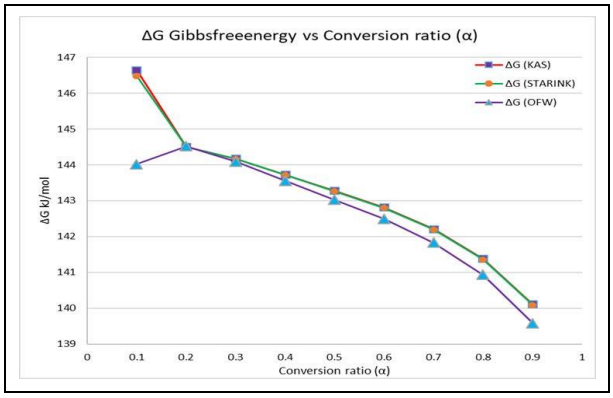

Fig. 19: Gibbs free energy vs conversion ratio comparison

OFW: The values for ΔS, ΔH, and ΔG for OFW also vary across different conversion rates. For example, at a conversion rate of 0.1, ΔS is approximately -0.251, ΔH is -23.224 kJ/mol, and ΔG is 144.019 kJ/mol. The average values for OFW indicate an average ΔS of -0.006, an average ΔH of 140.428 kJ/mol, and an average ΔG of 142.674 kJ/mol. Starink: Similar to the previous methods, Starink also shows variations in ΔS, ΔH, and ΔG with different conversion rates. For example, at a conversion rate of 0.1, ΔS is approximately -0.270, ΔH is -33.632 kJ/mol, and ΔG is 146.487 kJ/mol. The average values for Starink indicate an average ΔS of -0.022, an average ΔH of 129.015 kJ/mol, and an average ΔG of 143.178 kJ/mol. The values of ΔS, ΔH, and ΔG vary among the methods and fluctuate with the degree of conversion. The average values of ΔH, ΔS, and ΔG are determined to be 132.661, -0.01712, 143.019 kJ/mol.

Table 4. Kinetic parameters comparison

Conversion rate	KAS			OFW			Starink		
	ΔSS	ΔHH	ΔGG	ΔSS	ΔHH	ΔGG	ΔSS	ΔHH	ΔGG
0.1	-0.27079	-34.0656	146.6459	-0.2506	-23.2241	144.0191	-0.2699	-33.6316	146.487
0.2	-0.06508	98.84677	144.5034	-0.04848	110.503	144.5223	-0.06442	99.31235	144.5035
0.3	-0.01856	130.922	144.1753	-0.00184	142.7362	144.0931	-0.01789	131.3959	144.1715
0.4	-0.00453	140.4295	143.7282	0.012315	152.3518	143.5523	-0.00386	140.9034	143.7208
0.5	0.005717	147.3667	143.2762	0.022659	159.3721	143.0254	0.006398	147.8489	143.2657
0.6	0.013906	152.8935	142.8162	0.030927	164.9654	142.4978	0.014586	153.3757	142.8031
0.7	0.026051	161.2442	142.2128	0.04316	173.3909	141.8331	0.026743	161.7347	142.1971
0.8	0.042195	172.426	141.3793	0.059385	184.6476	140.9356	0.042885	172.9165	141.3611
0.9	0.062894	186.7839	140.113	0.080209	199.1135	139.5832	0.063595	187.2827	140.0913
Average	**-0.02313**	**128.5385**	**143.2056**	**-0.00581**	**140.4285**	**142.6735**	**-0.02243**	**129.0154**	**143.1779**

3.5 Blend Properties

Various tests were carried out on the bio-oil-diesel blend to determine its properties (Table 5). Flash Point (℃): The pyrolysis of oil-diesel blend exhibits a flash point of 54℃, which is within the range of 52-96℃ for diesel fuels. Fire Point (℃): The fire point of the pyrolysis oil-diesel blend was measured at 62℃, indicating a slightly higher fire point than the standard range of 55-100℃ for diesel fuels.

The density of the pyrolysis oil-diesel blend was 0.82 g/cc, which is lower than the typical range of 0.835-0.88 g/cc observed for diesel fuels. The kinematic viscosity of the pyrolysis oil-diesel blend was 2.61 centistokes, slightly higher than the range 2-4.5 centistokes commonly found in diesel fuels. The dynamic viscosity of the pyrolysis oil-diesel blend was 3.18 centipoise. The calorific value of pyrolysis oil-diesel blend was 22.68 MJ/kg, significantly lower than the range 42.5-45.5 MJ/kg typically seen in diesel fuels.

Table 5. Comparison of properties of oil blend with diesel

Fuel	Pyrolysis oil-Diesel Blend	Diesel fuel
Flash point (℃)	54	52- 96
Fire point (℃)	62	55-100
Density (g/cc)	0.82	0.835-0.88
Kinematic viscosity (centistokes)	2.61	2-4.5
Dynamic viscosity (centipoise)	3.18	2.5-5

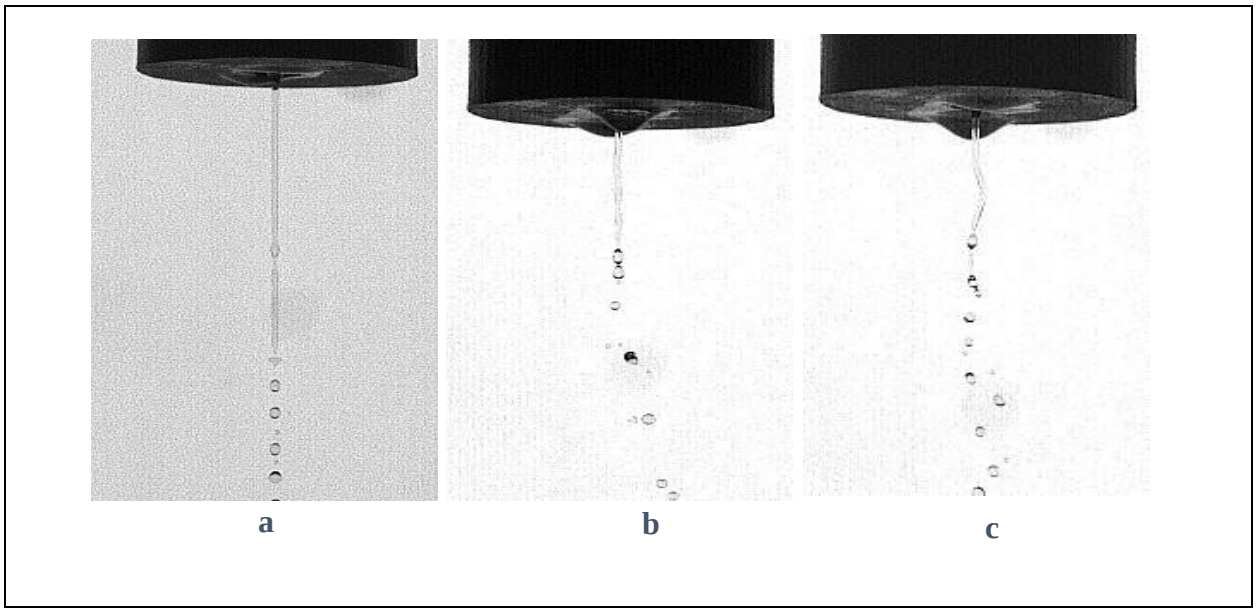

Fig. 20: Jet breakup at: (a) Zero air velocity, (b) Air velocity= 4.95 m/s, (c) Air velocity =5.03 m/s, Liquid velocity = 0.11 m/s

3.6 Image Sequence (Qualitative)

Fig. 20 and 21 show images captured at 10,000 fps for various air velocities as labelled. Breakup Length: The breakup length refers to the distance along the axis of a spray where the liquid fuel jet undergoes fragmentation, breaking up into smaller droplets. It serves as a measure of the spatial extent of primary atomization. As shown in Fig. 21(a), the breakup length is typically determined by analyzing spray images or conducting experimental measurements. It provides valuable insights into the atomization process and the size distribution of the resulting droplets. Spray Angle: The spray angle represents the cone-shaped spread of the spray plume as it emerges from the nozzle. It is defined as the angle formed between the outer edges of the spray cone. The spray angle can vary depending on factors such as nozzle design, operating conditions, and fluid properties. As shown in Fig. 21(b), it is a crucial parameter in applications where the coverage area or directionality of the spray is significant, such as in agricultural spraying, fuel injection, or coating processes.

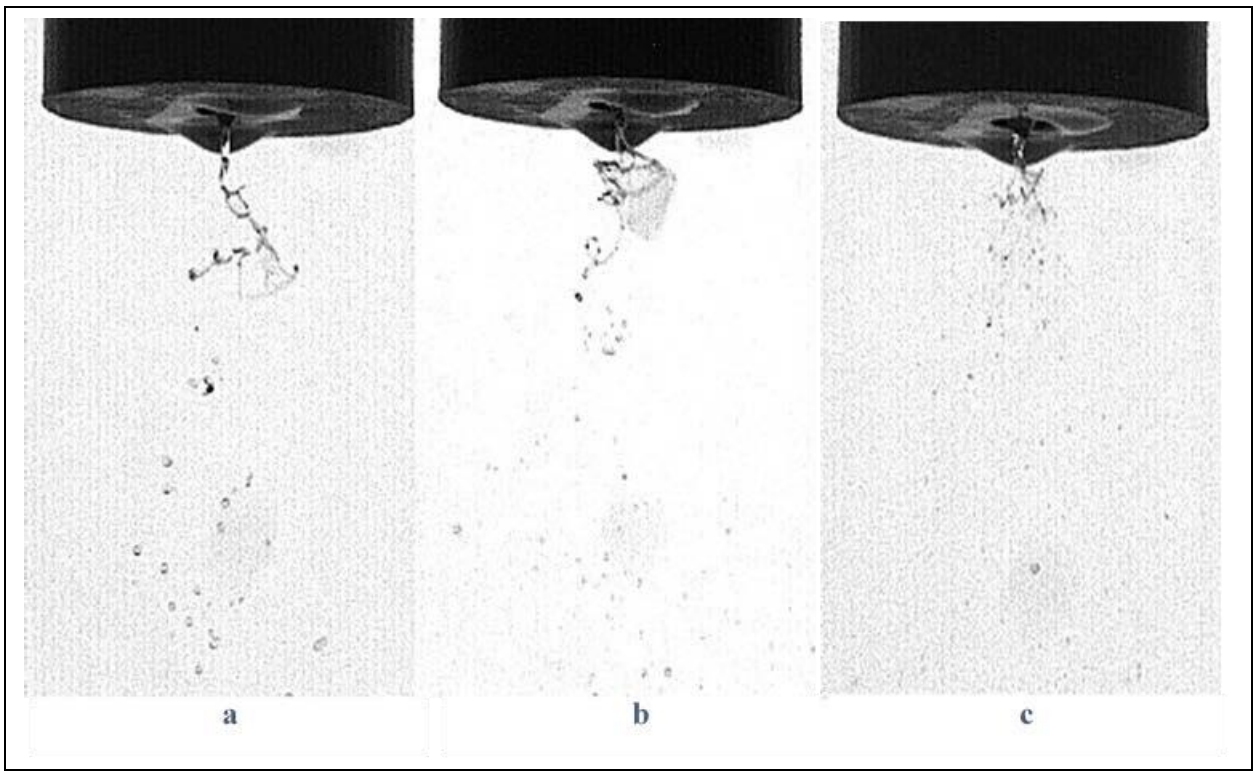

Fig. 21: Jet breakup at: (a) Zero air velocity, (b) Air velocity = 4.95 m/s, (c) Air velocity = 5.03 m/s, Liquid velocity = 0.11 m/s

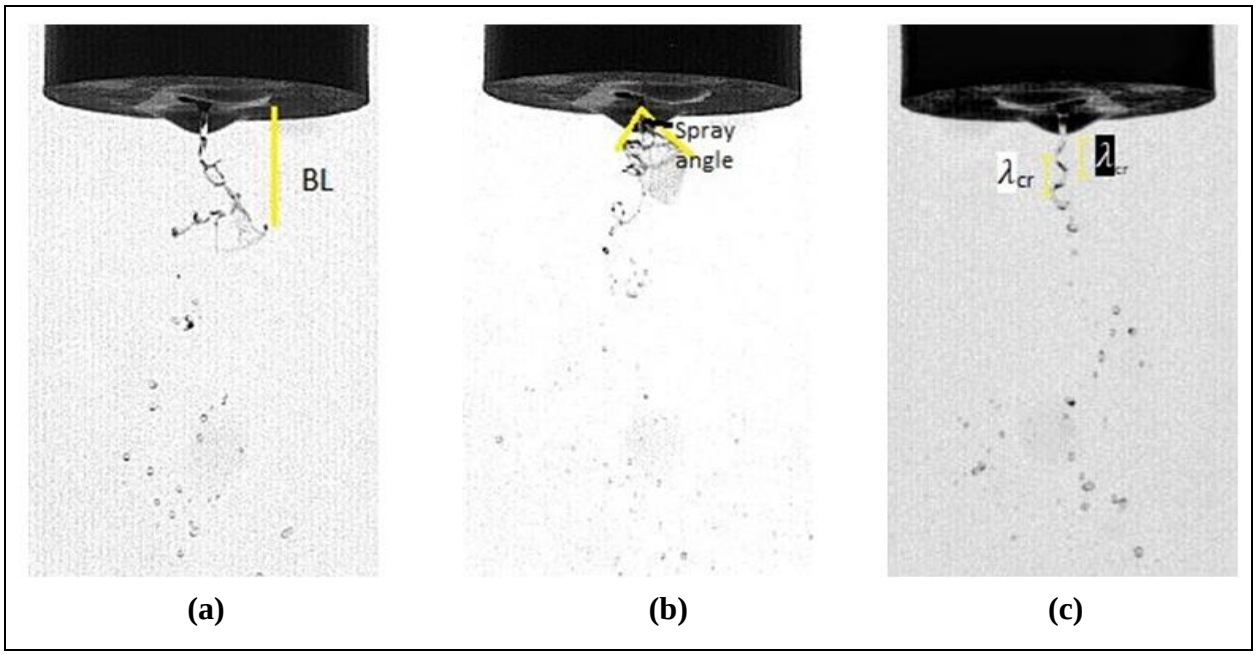

Fig. 22: (a) Breakup length, (b) Spray angle (c) Critical wavelength

As shown in Fig. 21(c), the critical wave number, also known as the most amplified wavelength or dominant wavelength, characterizes the instability of a liquid jet or spray. It is associated with the growth rate of disturbances within the spray. The critical wave number can be determined using stability analysis techniques or by examining the spatial and temporal characteristics of the spray. Understanding the critical wave number aids in predicting the breakup behavior and dispersion patterns of the spray. The value of critical wavelength is determined to be 4.184 mm (Fig. 22).

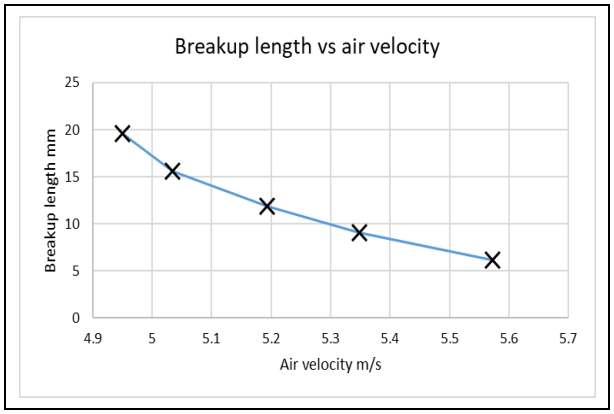

Fig. 23: Breakup length as a function of air velocity

Fig. 23 shows values of breakup length estimated from imaging software at various air velocities. At an air velocity of 0 m/s, the corresponding breakup length is 41.012 mm. As the air velocity increases, the breakup length generally decreases. For example, at an air velocity of 4.95 m/s, the breakup length is 19.547 mm, and at 5.57 m/s, the breakup length reduces to 6.107 mm. The data shows a decreasing trend in the breakup length with increasing air velocity, indicating that higher air velocities tend to cause smaller breakup lengths.

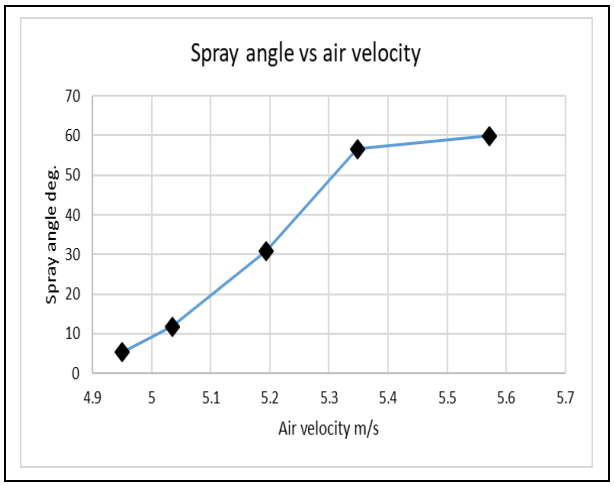

Fig. 24: Spray angle as a function of air velocity

Fig. 24 shows a plot for spray angle values. At an air velocity of 0 m/s, the spray angle is measured as 1.426°. As the air velocity increases, the spray angle tends to rise as well. For example, when the air velocity reaches 4.95 m/s, the spray angle expands to 5.368°. Furthermore, at 5.57 m/s, the spray angle significantly increases to 59.944°. The data clearly illustrates a positive correlation between air velocity and spray angle, indicating that higher air velocities lead to larger spray angles. Fig. 25 shows variation of breakup frequency with air velocities. At an air velocity of 4.95 m/s, the corresponding breakup frequency is 588.23 Hz. As the air velocity increases, the breakup frequency generally decreases. For example, at an air velocity of 5.57 m/s, the breakup frequency reduces to 178.571 Hz. The data shows a decreasing trend in the breakup frequency with increasing air velocity, indicating that higher air velocities tend to result in lower breakup frequencies.

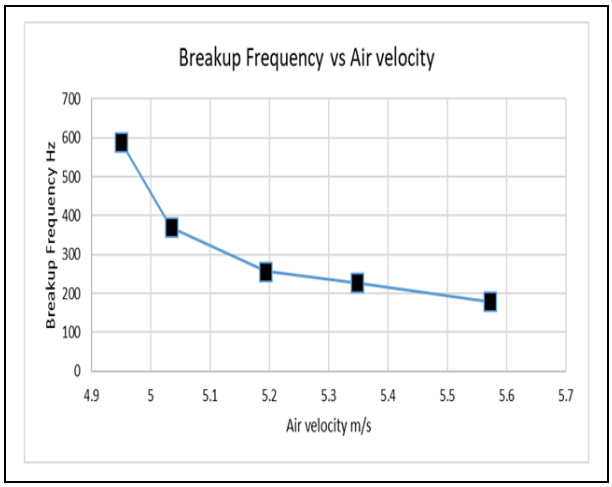

Fig. 25: Breakup frequency vs air velocity

4. CONCLUSIONS

The breakdown of face masks begins at a temperature of about 400 ℃ and ends at around 500 ℃ for linear heating rates of 5, 10, 15, and 20 ℃/min. Facemasks pyrolyze at temperatures between 450 and 470 degrees. The activation energy of decomposition process was investigated through a chemical kinetic study employing three different methods: Kissinger-Akahira-Sunose, Ozawa-Flynn-Wall, and the Starink model. Thermodynamic properties such as enthalpy, entropy, and Gibbs free energy were determined to be 132.661, -0.01712, and 143.019 kJ/mol, respectively. The activation energy values for the KAS, OFW, and Starink models were found to be 178.17, 190.06, and 178.67 kJ/mol, respectively. According to the ultimate and proximate analyses, the volatile content was quite high (94.07%), and the element with the greatest carbon content (83.78%) is carbon.

Use of surfactant as a catalyst in blending proves to be an effective method to create homogenous blends. FTIR analysis proves useful in interpretation of presence of various functional groups in the oil and char. Miniature atomizer can be used for spray characterization. The properties of the bio-oil and diesel blend are similar to that of petroleum diesel. The pyrolysis oil-diesel blend exhibits distinct properties compared to conventional diesel fuels. It has a slightly higher flash point and fire point, but has a low density. Additionally, the blend has slightly higher kinematic and dynamic viscosities. However, it is important to note that the blend shows significantly lower calorific value. These differences in properties should be taken into consideration when

evaluating the feasibility and efficiency of using pyrolysis oil-diesel blend as an alternative fuel.

Breakup length goes on decreasing with increase in the air velocity whereas spray angle increases with increasing air velocity. The breakup frequency results show decreasing trend in the breakup frequency with increasing air velocity, indicating that higher air velocities tend to result in lower breakup frequencies. As there are very limited studies in the field of high-speed flow visualization of bio-diesel blends, this study is unique and novel for atomization of advanced synthetic fuels which scopes further into waste to energy conversion studies. The utilization of advanced synthetic fuel, specifically the pyrolysis oil-diesel blend derived from facemasks, holds promising potential as an energy source within the waste-to-energy framework.

FUNDING

This research received no specific grant from any funding agency in the public, commercial, or not-for-profit sectors.

CONFLICTS OF INTEREST

The authors declare that there is no conflict of interest.

COPYRIGHT

REFERENCES

Akbulut, G. and Yalniz, Ş. Ç., Impact of Covid-19 Pandemic on Public Aquariums in Turkey, *Natural and Engineering Sciences*, 7(3), 260-270 (2022). https://doi.org/10.28978/nesciences.1221627

Amiruzzaman, M., Islam, M. R., Islam, M. R. and Nor, R. M. Analysis of COVID-19: An infectious disease spread. *J. Internet Serv. Inf. Secur.*, 12(3), 1-15 (2022). https://doi.org/10.22667/JISIS.2022.08.31.001

Aragaw, T. A. and Mekonnen, B. A., Current plastics pollution threats due to COVID-19 and its possible mitigation techniques: a waste-to-energy conversion via Pyrolysis, *Environ. Syst. Res.*, 10(8), 1-11 (2021). https://doi.org/10.1186/s40068-020-00217-x

Asadullah, M., Ab Rasid, N. S., Kadir, S. A. S. A. and Azdarpour, A., Production and detailed characterization of bio-oil from fast pyrolysis of palm kernel shell, *Biomass Bioenerg Journal*, 59, 316-324 (2013). https://doi.org/10.1016/j.biombioe.2013.08.037

Azam, M. A., Loo, J., Khan, S. K. A., Naeem, U., Adeel, M. and Ejaz, W., Behavioural patterns analysis of low entropy people using proximity data, *J. Wirel. Mob. Netw. Ubiquitous Comput. Dependable Appl.*, 3(3), 21-40 (2012).

Balaji, K., Sivadas, V., Radhakrishna, V., Ashok Bhatija, K. and Sai Charan, K., Experimental Characterization of Intrinsic Properties Associated with Air-Assisted Liquid Jet and Liquid Sheet, *J. Fluids Eng.*, 140(5), 051301 (2018). https://doi.org/10.1115/1.4038759

Clifford Ishola, B., Ojokuku, Y., Akpobasah-Amugen, S. and Eluyemi, O., Library Services Amidst the COVID-19 Pandemic: Study of Remotely Exploitable Electronic Academic Databases in Selected University Libraries in Nigeria, *Indian Journal of Information Sources and Services*, 13(1), 49–54 (2023).

Criado, J., Sánchez-Jiménez, P. and Pérez-Maqueda, L., Critical study of the isoconversional methods of kinetic analysis, *J. Therm. Anal. Calorim.*, 92(1), 199-203 (2008). https://doi.org/10.1007/s10973-007-8763-7

Ebnesajjad, S., Surface and material characterization techniques, *Handbook of adhesives and surface preparation*, *William Andrew Publishing*, 31-48 (2011). https://doi.org/10.1016/B978-1-4377-4461-3.10004-5

Ghasemi, A., Li, X., Hong, Z. and Yun, S., Breakup mechanisms in air-assisted atomization of highly viscous pyrolysis oils, *Energy Convers. Manag.*, 220, 113122 (2020). https://doi.org/10.1016/j.enconman.2020.113122

Harussani, M. M., Sapuan, S. M., Rashid, U., Khalina, A. and Ilyas, R. A., Pyrolysis of polypropylene plastic waste into carbonaceous char: Priority of plastic waste management amidst COVID-19 pandemic, *Sci. Total Environ.*, 803, 149911 (2022). https://doi.org/10.1016/j.scitotenv.2021.149911

Jahirul, M. I., Rasul, M. G., Chowdhury, A. A. and Ashwath, N., Biofuels production through biomass pyrolysis—a technological review, *Energies*, 5(12), 4952-5001 (2012). https://doi.org/10.3390/en5124952

Khachani, M., El Hamidi, A., Kacimi, M., Halim, M. and Arsalane, S., Kinetic approach of multi-step thermal decomposition processes of iron (III) phosphate dihydrate FePO4·2H2O, *Thermochim. Acta*, 610, 29-36 (2015). https://doi.org/10.1016/j.tca.2015.04.020

Kristanto, J., Azis, M. M. and Purwono, S., Multi-distribution activation energy model on slow pyrolysis of cellulose and lignin in TGA/DSC, *Heliyon*, 7(7), E07669 (2021). https://doi.org/10.1016/j.heliyon.2021.e07669

Li, C., Yuan, X., Sun, Z., Suvarna, M., Hu, X., Wang, X. and Ok, Y.S., Pyrolysis of waste surgical masks into liquid fuel and its life-cycle assessment, *Bioresour. Technol.*, 346, 126582 (2022). https://doi.org/10.1016/j.biortech.2021.126582

Mangesh, V. L., Padmanabhan, S., Tamizhdurai, P., Narayanan, S. and Ramesh, A., Combustion and emission analysis of hydrogenated waste polypropylene pyrolysis oil blended with diesel, *J. Hazard. Mater.*, 386, 121453 (2020). https://doi.org/10.1016/j.jhazmat.2019.121453

Martynis, M., Winanda, E. and Harahap, A. N., Thermal pyrolysis of polypropylene plastic waste into liquid fuel: reactor performance evaluation, *IOP Conf. Ser. Mater. Sci. Eng.*, 543(1), 012047 (2019). https://doi.org/10.1088/1757-899X/543/1/012047

Matsuzawa, Y., Ayabe, M. and Nishino, J., Acceleration of cellulose co-pyrolysis with polymer, *Polym. Degrad. Stab.*, 71(3), 435-444 (2001). https://doi.org/10.1016/S0141-3910(00)00195-6

Minov, S. V., Cointault, F., Vangeyte, J., Pieters, J. G. and Nuyttens, D., Pesticide spray characterisation using high speed imaging techniques, *Agric Agric Sci Proc.*, 7, 280-286 (2015). https://doi.org/10.1016/j.aaspro.2015.12.048

Mondal, S., Environmental catastrophe amidst covid-19 pandemic: Disposal and management of PPE kits for the production of biofuel with the sustainable approach in solar thermal energy, *Mater. Today Proc.*, 64, 1266-1271 (2022). https://doi.org/10.1016/j.matpr.2022.03.721

Nandiyanto, A.B.D., Oktiani, R. and Ragadhita, R., How to read and interpret FTIR spectroscope of organic material, Indonesia, *J. Sci. Technol.*, 4(1), 97-118 (2019). http://dx.doi.org/10.17509/ijost.v4i1.15806

Nasrollahzadeh, M., Atarod, M., Sajjadi, M., Sajadi, S.M. and Issaabadi, Z., Plant-mediated green synthesis of nanostructures: mechanisms, characterization, and applications, *Interface Sci. Tech.*, 28, 199-322 (2019). https://doi.org/10.1016/B978-0-12-813586-0.00006-7

Nileshkumar, K.D., Jani, R.J., Patel, T.M. and Rathod, G.P., Effect of blend ratio of plastic pyrolysis oil and diesel fuel on the performance of single cylinder CI engine, *Int. J. Sci. Technol. Eng.*, 1(11), 195-203 (2015).

Panchasara, H. and Ashwath, N., Effects of pyrolysis bio-oils on fuel atomisation—a review, *Energies*, 14(4), 794 (2021). https://doi.org/10.3390/en14040794

Park, C., Choi, H., Lin, K.Y.A., Kwon, E.E. and Lee, J., COVID-19 mask waste to energy via thermochemical pathway: Effect of Co-Feeding food waste, *Energy*, 230, 120876 (2021). https://doi.org/10.1016/j.energy.2021.120876

Qureshi, M.S., Oasmaa, A., Pihkola, H., Deviatkin, I., Tenhunen, A., Mannila, J., Minkkinen, H., Pohjakallio, M. and Laine-Ylijoki, J., Pyrolysis of plastic waste: Opportunities and challenges, *J Anal Appl Pyrol.*, 152, 104804 (2020). https://doi.org/10.1016/j.jaap.2020.104804

Sakthivel, R., Tamilarasan, N., Kumar, P.S., Hari, S.D.S., Mathesh, V. and kumar, S.P., Kinetic and thermodynamic analysis of Borassus flabellifer bark pyrolysis for effective production of biofuel, *Biomass Convers, Biorefin.*, 1-10 (2023). https://doi.org/10.1007/s13399-023-04699-4

Salin, I.M. and Seferis, J.C., Kinetic analysis of high-resolution TGA variable heating rate data, *J. Appl. Polym. Sci.*, 47(5), 847-856 (1993). https://doi.org/10.1002/app.1993.070470512

Sharma, H.B., Vanapalli, K.R., Cheela, V.S., Ranjan, V.P., Jaglan, A.K., Dubey, B., Goel, S. and Bhattacharya, J., Challenges, opportunities, and innovations for effective solid waste management during and post COVID-19 pandemic, *Resour. Conserv. Recycl.*, 162, 105052 (2020). https://doi.org/10.1016/j.resconrec.2020.105052

Stevovic, I., Hadrović, S., & Jovanović, J., Environmental, social and other non-profit impacts of mountain streams usage as Renewable energy resources, *Arch Tech Sci.*, 2(29), 57-64 (2023). http://dx.doi.org/10.59456/afts.2023.1529.057S

Sun, X., Liu, Z., Shi, L. and Liu, Q., Pyrolysis of COVID-19 disposable masks and catalytic cracking of the volatiles, *J Anal Appl Pyrol.*, 163, 105481 (2022). https://doi.org/10.1016/j.jaap.2022.105481

Szwarc, M., The kinetics of the thermal decomposition of propylene, *J. Chem. Phys.*, 17(3), 284-291 (1949). https://doi.org/10.1063/1.1747240

Tamilarasan, N., Sakthivel, R. and Balaji, K., and Hoang, A.T., High efficient COVID-19 waste co-pyrolysis char/TiO_2 nanocomposite for photocatalytic reduction of Cr (VI) under visible light, *Environ. Sci. Pollut. Res. Int.*, 30(43), 97178-97194 (2023). https://doi.org/10.1007/s11356-023-29281-3

Tamilarasan, N., Sakthivel, R. and Balaji, K., Influence of metal oxide catalyst on co-pyrolysis of biomass and COVID-19 waste, *Environ. Technol.*, 1721-1732 (2022). https://doi.org/10.1080/09593330.2022.2151941

Yousef, S., Eimontas, J., Stasiulaitiene, I., Zakarauskas, K. and Striūgas, N., Pyrolysis of all layers of surgical mask waste as a mixture and its life-cycle assessment, *Sustain. Prod. Consum.*, 32, 519-531 (2022). https://doi.org/10.1016/j.spc.2022.05.011

Yousef, S., Eimontas, J., Striūgas, N. and Abdelnaby, M.A., Pyrolysis kinetic behaviour and TG-FTIR-GC–MS analysis of coronavirus face masks, *J. Anal. Appl. Pyrol.,* 156, 105118 (2021). https://doi.org/10.1016/j.jaap.2021.105118